

J. Environ. Treat. Tech. ISSN: 2309-1185

Journal web link: https://dormaj.org/index.php/jett https://doi.org/10.47277/JETT/10(1)9



Exploring the Photocatalytic Activity of Mn & Al Incorporated MCM-41 towards the Removal of Rhodamine B and Congo Red Dyes under Visible Light and their Kinetic Study

Jayarangarao Prathipati 1,2, Paul Douglas Sanasi 2*

¹ Department of Chemistry, Baba Institute of Technology & Sciences (BITS), Visakhapatnam-530041, Andhra Pradesh, India ² Department of Engineering Chemistry, AU College of Engineering (A), Andhra University, Visakhapatnam-530003, Andhra Pradesh, India

Abstract

Manganese and Aluminum incorporated mesoporous silica materials (Mn & Al-MCM-41) were synthesized using the co-precipitation method. They have been characterized using XRD, SEM-EDX, FTIR, surface area (S_{BET} , $m^2.g^{-1}$), and UV-Vis DRS spectral studies. The spectral analysis explored that the mesoporosity was retained even after the acid functionalization of materials. There was a significant fall in the surface area (S_{BET} , $m^2.g^{-1}$), pore size (Å), and pore volume (cc. g^{-1}) on merging Mn and Al atoms into the skeleton of MCM-41. Their light absorption was found to be profound in the visible light as observed from the UV-Vis DRS analysis, and pertaining to these results, their suitability as photocatalysts were examined towards the oxidative removal of a *xanthene* (Rhodamine B) and an *azo* dye (Congo red). Scavengers experiment revealed that both OH• (hydroxyl radicals) and O_2 • (superoxide radical ions) were the active oxidative species in the removal of the dyes. In the kinetic profile analysis, the rate of removal of the dyes was found to meet the Langmuir-Hinshelwood (L-H) kinetic model.

Keywords: Mesoporous silica, Photocatalysis, Scavengers, Rhodamine B, Congo Red

1 Introduction

The chemistry of mesoporous silica molecular sieves, M41S, was initiated from 1991 to 1992 by the Mobil scientists [1-3]. Since their discovery, these materials have been synthesized in different methods and their applicability was evaluated for catalysis, adsorption, separating bulk molecules, producing onepot organic derivatives, pollutants removal, etc. [4, 5]. In the family of M41S materials, MCM-41 was known to possess a regular hexagonal array of uniform pores with 2-10 nm of diameter range. These hexagonal MCM-41 materials were identified to be materials of research interest, due to their high specific area, thermal and hydrothermal stability, and potential adsorbents [6, 7]. However, the applications of their purest form were limited due to the existence of the neutral scaffold of the molecular sieves [7]. To extend their usage in different scientific fields, the materials can be modified by integrating with different heteroatoms. The MCM-41 materials were inserted with various d-block metals ions like Ti, V, Mn, Fe, Co, Cu, Zn, Zr, etc and a few p-block elements like B, Al, Ga, etc and form Metallo-silicate molecular sieves, that can be used in different applications [8-23]. In these modified forms, the Si atom undergoes isomorphous substitution and possesses acidic sites due to which they display superior catalytic activity in the selective oxidation process and organic transformations [24, 25]. In the view of environmental sustainability, metal incorporated MCM-41 materials can be used as photocatalysts to degrade the hazardous industrial effluents released into the environmental wastewaters [24].

The main aim of this research is to synthesize Mn & Al incorporated MCM-41 molecular sieves with a facile coprecipitation method. These acid-functionalized mesoporous materials were applied as photocatalysts for the destruction of Rhodamine B and Congo red dyes in their aqueous solutions under visible light illumination. The supporting experimental factors like the role of scavengers, the effect of initial dye concentration, the weight of photocatalyst, pH were studied and represented along with their kinetic profiles.

2 Experimental

2.1 Materials and Methods

Cetyltrimethylammoniumbromide (CTAB, $C_{16}H_{33}(CH_3)_3N^+Br^-$) Tetraethylorthosilicate (TEOS), Manganese (III) acetylacetonate, and Aluminum (III) Isopropoxide and were

¹*Corresponding author: Paul Douglas Sanasi (ORCID: 0000-0002-5839-0959), Department of Engineering Chemistry, AU College of Engineering (A), Andhra University, Visakhapatnam-530003, Andhra Pradesh, India. Email: pauldouglas12@gmail.com

procured from Sigma Aldrich, ammonia (25 %), and ethyl alcohol was obtained from SRL laboratories, India and was used without further purification. Rhodamine B ($C_{28}H_{31}ClN_2O_3$, MW = 479.02 g/mol) and Congo red ($C_{32}H_{22}N_6Na_2O_6S_2$, MW = 696.665 g/mol) were chosen as the probe molecules for the study of their removal with the synthesized mesoporous materials. All the solutions were prepared by using double distilled water (DI).

2.2 Synthesis of Mn & Al-MCM-41 materials

A simple co-precipitation method was conducted to prepare metal incorporated MCM-41 materials under ambient conditions of temperature and quantity of surfactant [7]. These mesoporous materials were synthesized by dissolving the surfactant, CTAB (2.4 g) in 120 mL of DI and kept under magnetic stirring at room temperature until a homogenous solution was formed. To this solution, 10.2 mL of aq. Ammonia (25 wt.%) was added under stirring conditions. At this stage, silica precursor, TEOS was added slowly dropwise and the resultant solution turned into milky precipitate and on a long-standing, a gel formation has observed due to the hydrolysis of the silica precursor.

To obtain Mn and Al-MCM-41 materials, their precursors' Manganese acetylacetonate [Mn(acac)₃] and Aluminium Isopropoxide [Al(iso-C₃H₇)₃] was added to this gel in a ratio of Si:M = 100: 1(M=Mn, Al) (Figure 1). After their addition in two separate synthetic vessels, the gel formed was further kept to stirring for about 2 hours to get complete hydrolysis of TEOS and proper incorporation of the target metals into the mesoporous MCM-41. The so obtained white precipitates were filtered and washed thoroughly with DI and EtOH, separately. Both the products were dried at around 110-120 °C overnight. At last, the solid products were sintered near 550 °C in the air atmosphere for 5 hours, to remove the surfactant. Similarly, free MCM-41 was synthesized without the metal precursors.

2.3 Characterization

The mesoporous materials have been characterized as follows. The X-ray diffraction patterns were recorded using Philips X'Pert X-ray diffractometer (air atmosphere, room temperature) supported with Cu K_{α} ($\lambda=1.5406~A^{\circ}$) radiation operating at 40 kV and 40 mA, with 20 angle varying from $0.5^{\circ}-10^{\circ}$ with a scan speed of $0.02^{\circ}~s^{-1}$. Philips XL 30 SEM scanning electron microscope (FEI-Philips, Hillsboro) was used to record the FESEM micrographs of the samples. Using a Quantachrome Nova 2000e surface area and pore size analyzer, the surface area, pore size, and volume were measured by N_2 adsorption-desorption (liquid N_2 atmosphere, 77 K). The optical properties of the mesoporous materials were investigated with a Single Monochromator UV-2600 (optional ISR-2600Plus, λ up to 1400 nm).

3 Results and Discussions

3.1 XRD analysis:

In the XRD patterns of the samples (Figures 2a, 2b), a high-intensity peak was observed at $2\theta = 2.1^{\circ}$. This characteristic peak designates the mesoporous nature in the long-range hexagonal moiety in MCM-41, corresponding to the diffraction plane d_{100} [8]. This value of 2θ also occurs due to the long carbon chain (C-19) used in their synthesis. There was no huge change in the position of the peak and the intensity of the XRD peaks, which shows that both Mn & Al-MCM-41 were formed in mesoporous nature as like in its parent template, MCM-41.

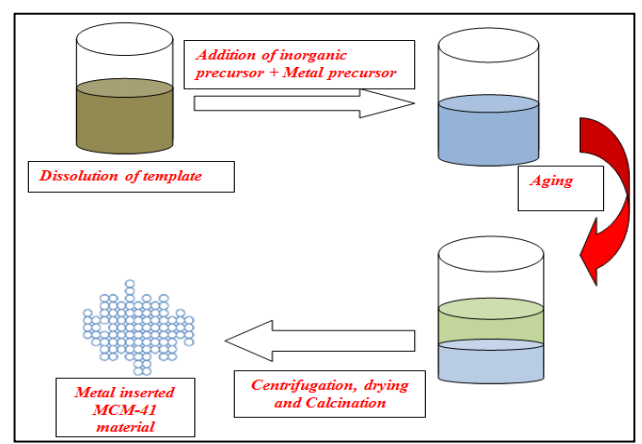


Figure 1: Synthesis of Mn & Al-MCM-41

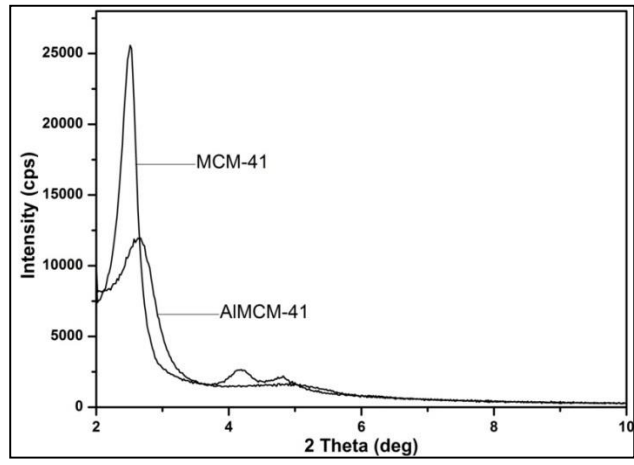


Figure 2a: XRD pattern of MCM-41 and Al-MCM-41

3.2 N₂ adsorption-desorption studies

Brunauer, Emmet, and Teller (BET) N_2 adsorption-desorption studies were carried out to analyze their surface area, pore size (PS), and volume (PV). The surface areas ($S_{\rm BET}$, $m^2.g^{-1}$) of the synthesized materials were found to decrease when compared with the parent material, MCM-41 (Table 1). The adsorption isotherms follow the typical type-IV adsorption isotherm which itself signifies the mesoporosity in the materials [26]. From the BJH (Barrett-Joyner-Halenda) plots of the pore volume and pore distribution, it was found that the pore size of the materials was in nanoscale. Similarly, there was a significant reduction in the values of PS and PV indicating the impact of Mn^{+3} and AI^{+3} ions in the MCM-41 materials.

Table 1: Results of N₂ adsorption-desorption studies

Material	S_{BET} , (m^2g^{-1})	PS, (Å)	PV, (cc g ⁻¹)	
Mn-MCM-41	786.1	18.9	0.21	
Al-MCM-41	856.2	17.3	0.20	
MCM-41	1023.01	22.2	0.28	

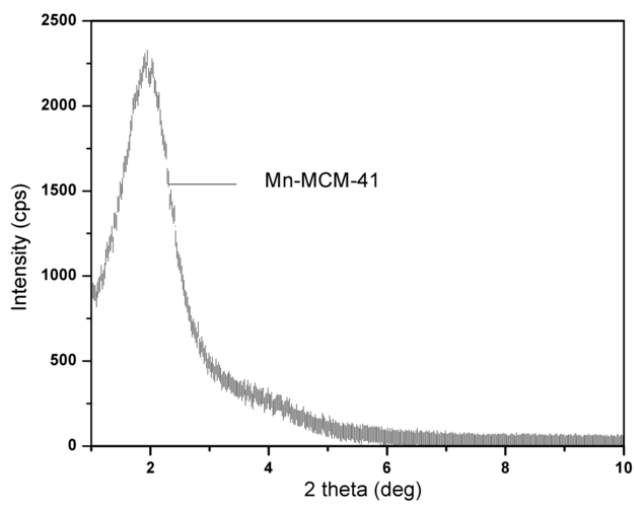


Figure 2b: XRD of Mn-MCM-41

3.3 FT-IR

The FT-IR spectra of Mn and Al-MCM-41 were represented in Figure 3. A low intense peak was obtained at 2926 cm⁻¹, representing the C-H stretching vibrations of the long-chain hydrocarbon in the CTAB (surfactant). The surface-attached silanols (Si-OH) and the adsorbed water molecules were identified by the broad peak obtained at near 3408 cm⁻¹. Near 1630 cm⁻¹, the absorption peaks were obtained representing the bending vibrations in the adsorbed water molecules. The absorption bands of Si-O-Si asymmetric stretching vibrations were observed at 1088 and 1235 cm⁻¹ respectively. The bending vibrations in the silanols band were observed at 962 cm⁻¹. The Si-O-Si bending vibrations can be attributed to the absorption peaks obtained in the range of 450 -795 cm⁻¹ [9]. In pure MCM-41 material, a band at 960 cm⁻¹ will be observed with high intensity and it corresponds to the presence of more silanol groups [9]. On insertion of the metal ions (Mn⁺³, Al⁺³), a similar peak (962-957 cm⁻¹) was obtained (Figure 3) with less intensity and they correspond to the presence of Si-O-M linkage (M=metal ions) in the mesoporous materials [27]. This might be due to a decrease in the number of silanol groups due to the incorporation of the metal ions into the mesoporous framework [9].

3.4 SEM-EDX analysis

The SEM-EDX images of MCM-41 and $M^{\rm III}$ -MCM-41 (M = Mn and Al) are shown in Figures 4a to 4d. The SEM micrographs of these materials represent the spherical-shaped particles, whose morphology was almost nearer to that present in MCM-41 (Figures 4a. 4c). EDX analysis confirms the presence of the respective elements (Si, O) along with the incorporated metal ions (Mn, Al) in the mesoporous materials (Figures 4b, 4d). The morphology in the materials did not change much on inserting the M^{+3} ions into the hexagonal array of MCM-41.

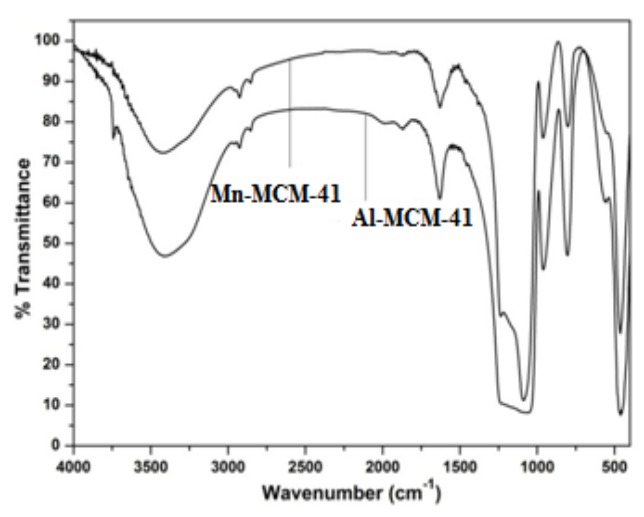


Figure 3: FT-IR spectra of Mn & Al-MCM-41

3.5 UV-Vis DRS analysis

The absorption maxima of the synthesized mesoporous materials were examined using UV-Vis DRS analysis and their results were presented in Figures 5a and 5b. It was found that Al⁺³ incorporated MCM-41 material has shown the wavelength maxima at around 580 nm (Fig. 5a). In Mn-MCM-41, Mn exhibits +III state (d⁴ configuration) and shows two absorption bands in the tetrahedral [$^5T_2(D) \rightarrow ^5E(D)$] and octahedral field [($^5E_g(D) \rightarrow ^5T_{2g}(D)$] [28]. Corresponding to these transitions, the material Mn-MCM-41 has shown an intense absorption peak near 635 nm and a less intense peak at around 530 nm respectively (Fig 5b). Concerning their absorption wavelengths, the bandgap energy (in electron volts, eV) was calculated using equation 1.

$$Eg = \frac{1240}{\lambda} \tag{1}$$

where λ is the wavelength in nanometers (nm). The observed bandgap energy was obtained as 2.13 eV for Al-MCM-41 and in Mn-MCM-41, it was obtained in the range 1.95 – 2.33 eV, corresponding to its two absorption maxima. These results reveal that the synthesized mesoporous materials possess a narrow band gap and could act as efficient photocatalysts in the visible region.

3.7 Photocatalytic removal studies

3.7.1 Absorption wavelength

It was observed that the aqueous solution of RhB absorbs at the wavelength maximum, $\lambda_{max} = 554$ nm and CR at $\lambda_{max} = 500$ nm. Using these absorption wavelengths, further studies were conducted. To measure these absorption wavelengths along with the absorptions of the experimental dyes samples collected at regular intervals, UV-Vis Spectrophotometer (Make: Shimadzu, wavelength range: 180-1100 nm) was used. The photocatalytic chamber was established by inserting a Tungsten halogen lamp (400 W, approximate wavelength range: 500-800 nm) into a wooden box, internally connected with a magnetic stirrer and water inlet, outlet source.

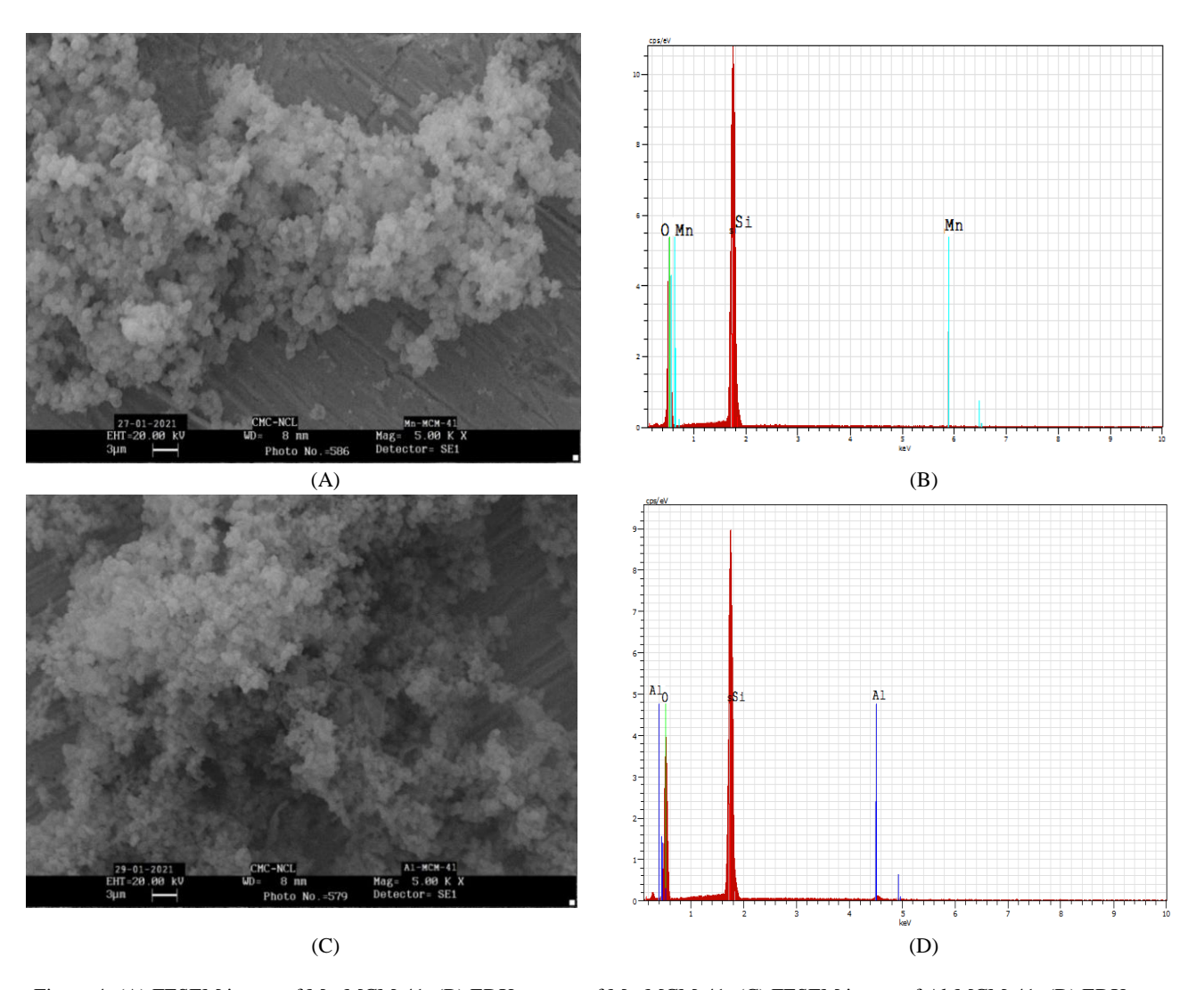


Figure 4: (A) FESEM image of Mn-MCM-41; (B) EDX spectra of Mn-MCM-41; (C) FESEM image of Al-MCM-41; (D) EDX spectra of Al-MCM-41

Aliquots from the dye sample solutions under investigation were collected at regular intervals and the samples were centrifuged to precipitate the mesoporous material. The supernatant liquid was examined for absorbance and the % removal of the dyes was calculated using equation 2.

% Removal of dye =
$$\frac{Co-Ct}{Co}$$
 x 100 (2)

where C_o and C_t are the initial concentration (ppm) of the dye sample (t=0 min) and concentration at a given time in min. The capacity of adsorption of the dyes on the surface of synthesized Mn & Al-MCM-41 mesoporous materials was studied by performing the adsorption isotherm experiment under dark conditions. From equation 3, the amount of dye adsorbed per unit mass of the mesoporous material, adsorbent (q_t , μ mol/g) at the time, t (min) was calculated [29].

$$q_t = \frac{(Co - Ct)V}{m} \tag{3}$$

where C_0 and C_t are the concentrations of the dye solutions ($\mu mol/L$) before and after adsorption respectively.

The volume (mL) of the dye solution and mass (mg) of the mesoporous material were denoted as V and m, respectively. The rate of adsorption of the dyes was plotted against time (min) as shown in figures 6a and 6b. It can be observed that rapid adsorption occurred for 30 min and 35 min of contact time for RhB and CR dyes respectively with both the metal-MCM-41 materials. The further adsorption phenomenon was almost negligible after these time intervals. From these results, it was optimized that the equilibration time was 30 min for RhB and 35 min for CR in the presence of mesoporous materials, and the same was maintained as the equilibration time for the upcoming experiments. In figures 6a, 6b, zone-I represents the increased rate of adsorption in the dark region and Zone-II represents the saturation levels of the adsorption of the dyes on the surface of the materials.

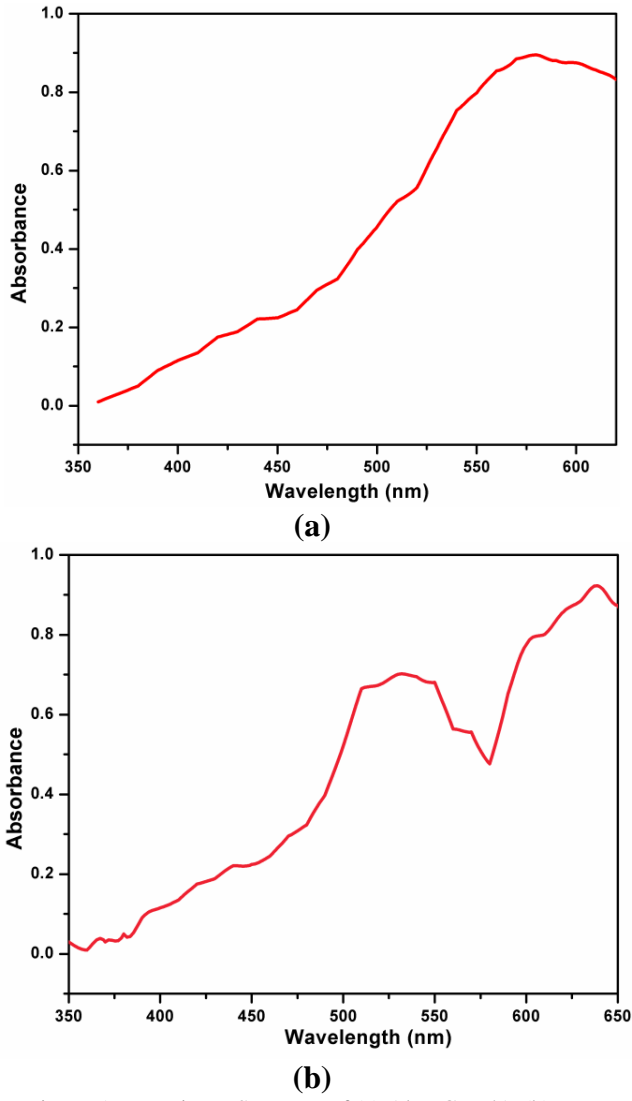


Figure 5: UV-Vis DRS spectra of (a) Al-MCM-41; (b) Mn-MCM-41

3.7.2 Effect of initial dye concentration

The concentration of the dyes solutions can influence the extent of their removal with the photocatalyst. Hence, the same was studied with the variable concentrations of both dyes and with a fixed weight of the mesoporous materials at their respective absorption wavelengths (Figures 7a, 7b). It was observed that the extent of their removal has grown up with the increase in the concentration of the dyes and at around 6-8 ppm and 8-10 ppm the degradation efficiency was maximum for the RhB (Figure 7a) and CR dyes (Figure 7b) with both the mesoporous materials respectively. Hence, these concentration limits were used as their optimum levels for the remaining experiments. On the other side of these limits, the rate of removal of the dyes was found to be minimum.

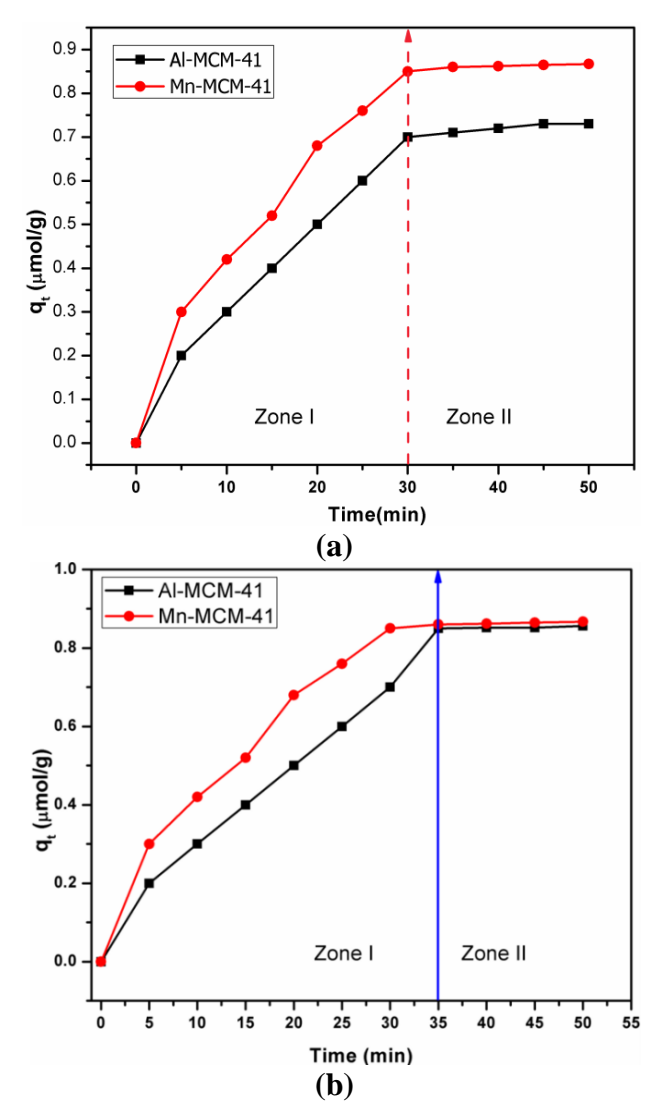


Figure 6: Adsorption studies: (a) RhB; (b) CR, with Mn and Al-MCM-41 materials

3.7.3 Effect of pH

The photocatalytic removal of RhB and CR dyes under visible light also depends on the pH of the medium and studies were performed using HCl (0.1 N) and NaOH (0.1 N). The chemical structure of RhB is pH sensitive (Figure 8) and in open-chain form, it exists in pink color (pH<7.0), and in closed lactone ring form it is colorless (pH>7.0) [30]. In order to study the color removal tendency, the pH of the dye was maintained at less than 7.0 (acidic), and in addition to this, on the incorporation of metal ions (Mn⁺³ and Al⁺³) into the mesoporous silica, the surface of the materials possess acid nature [12, 14]. Hence, on conducting the pH effect on the degradation efficiency of the RhB (from pH 2.0 – 8.0), it was observed that maximum removal was observed between 5.0-6.0 pH of the medium (0.1 N HCl). Mn & Al-MCM-41 have shown almost similar degradation tendency in this study (Fig. 9a).

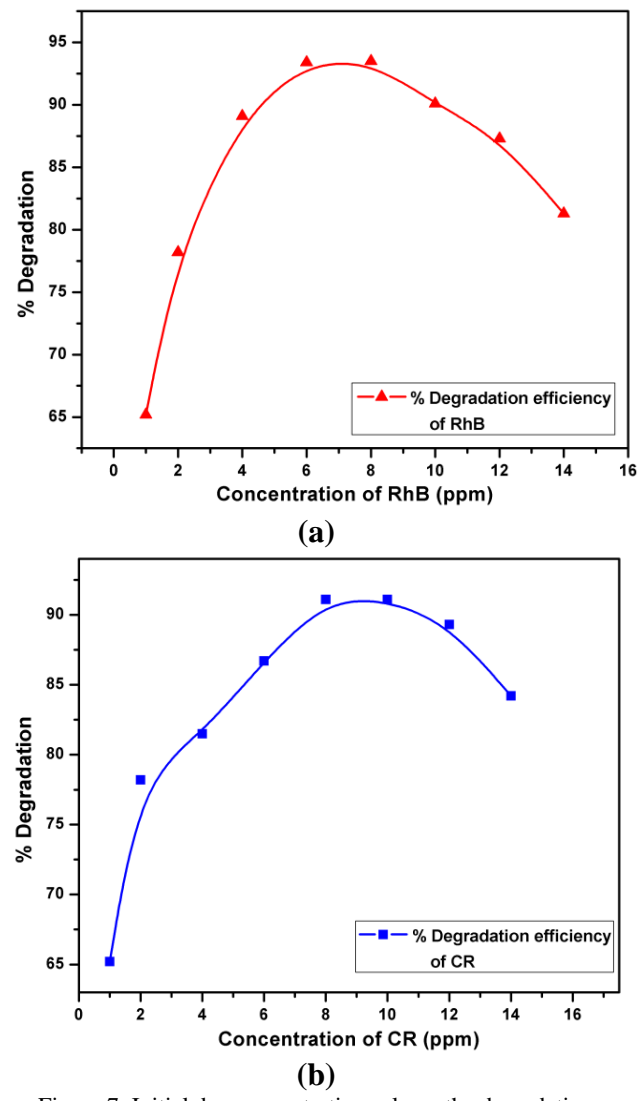


Figure 7: Initial dye concentration role on the degradation tendency; (a) RhB (b) CR with Mn & Al-MCM-41

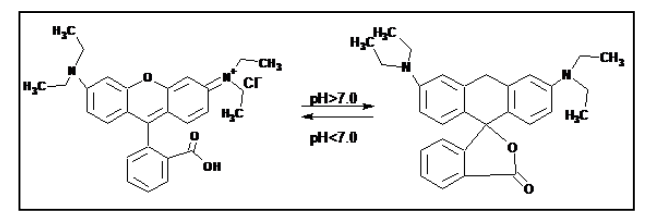


Figure 8: Chemical structures of RhB at different pH

Similarly, the degradation of CR dye with respect to the pH of the medium was studied. Congo red exhibits dark blue at below pH 3.0 and at above pH 5.2, it appears light to dark red [31]. As higher acidic mediums are not suggestible in environmental factors, (less than pH 3.0), the pH studies were conducted at above pH 5.2 by varying the pH from 5.0 to 10.0 with 0.1 N NaOH. With both the mesoporous materials, the removal of CR was maximum at around 8.0 to 9.0 pH. However, the removal tendency was

slightly higher with Mn-MCM-41 than with Al-MCM-41 (Figure 9b).

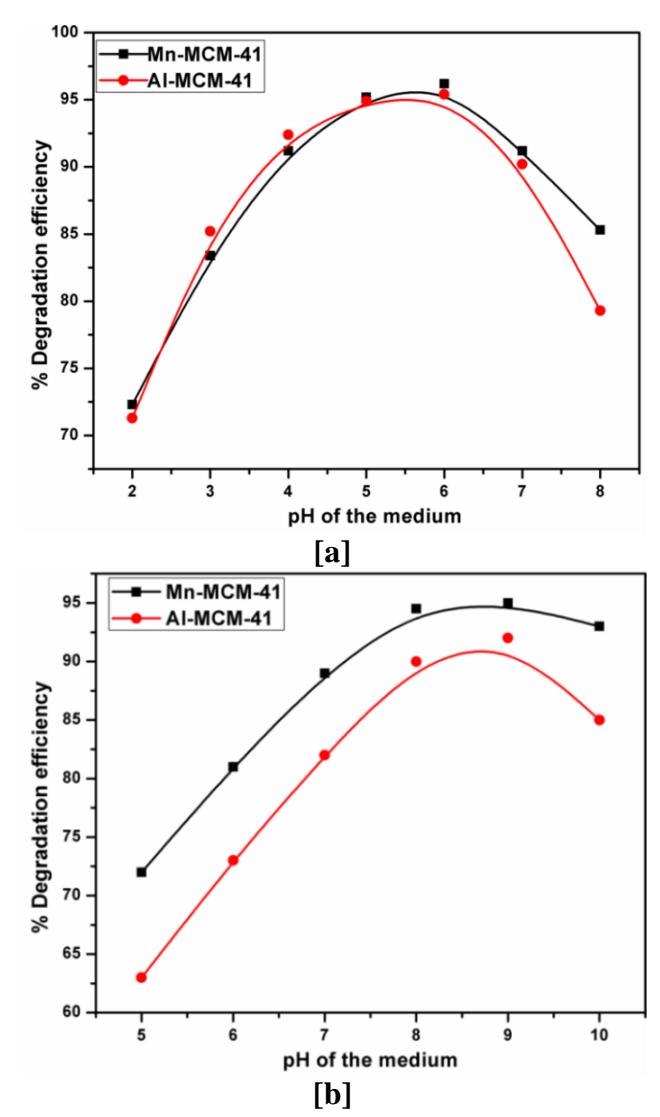


Figure 9. Effect of pH on the removal of (a) RhB; (b) CR

3.7.4 Influence of Mn and Al-MCM-41 and their composition towards the removal of RhB and CR dyes.

Using the above experimental factors, the influence of Mn and Al-MCM-41 materials in removing the RhB and CR dyes from their aqueous solution was examined and their results were presented in Figure 10 (a, b). It was observed that Mn-MCM-41 has removed the RhB and CR dyes in 90 and 60 min respectively. Whereas, Al incorporated samples have removed RhB in 100 min and CR dye in 75 min. In addition to these studies, the effect of the mesoporous material weight was studied separately and it was observed that the degradation tendency was maximum with 5-6 mg of Mn-MCM-41 and 8-9 mg of Al-MCM-41 materials in both the dyes. Outside this range, the tendency was less. Hence, from these studies, it was concluded that the mesoporous materials were efficient in removing the selected dyes in optimum time intervals, weight, and pH conditions.

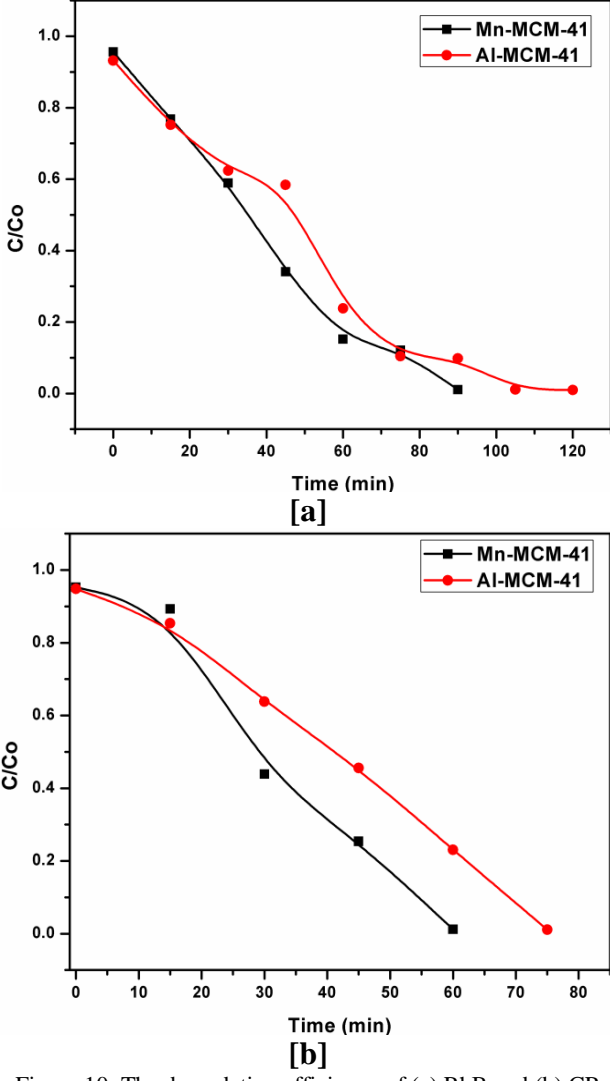


Figure 10: The degradation efficiency of (a) RhB and (b) CR dyes with the mesoporous materials

3.8 Kinetic studies

The kinetic profiles of the removal tendency of RhB and CR dyes were conducted using Langmuir-Hinshelwood (L-H) kinetic model [32].

$$r = dC/dt = kKC/(1 + KC)$$
 (4)

The equilibrium constant, $K_{\mathbb{C}}$ value can be neglected in the denominator (<<1), and on the integration of the above equation with time (t), it rearranges to pseudo-first-order rate equation as:

$$ln \frac{Co}{c} = kKt = k_{app}t$$
(5)

where Co and C are the initial concentration and concentration of the dye solutions at time t (min). kapp=k•K, where k is the rate constant (min⁻¹) and K is the coefficient of adsorption of the dyes onto the surface of mesoporous materials. Based on the rate of removal tendency of the dyes with MCM-41 along with its metal

ion incorporated mesoporous materials, the rate constants were calculated and presented in Table 2. It can be observed from the results, that the rate constants have increased nearly sixfold with Mn-MCM-41 and fivefold with Al-MCM-41 materials in comparison with the pure MCM-41 material. Hence, it was clear that the effect of Mn and Al over MCM-41 was highly effective in bringing out the photocatalytic removal of the dyes. Further, the removal tendency was slightly higher with Mn-MCM-41 its Aluminum analog, it might be due to the higher absorption wavelengths, and narrow bandgap in the former mesoporous material as observed from the UV-Vis DRS spectral analysis.

Table 2: Rate constants of removal efficiency of dyes with Mn & Al-MCM-41 materials

& Al-MCM-41 materials					
Dye/ Mesoporous	Rate constant with MCM-41	Rate constant with Mn-MCM-41	Rate constant with		
material	MCM 41	WIII WICHT 41	Al-MCM-41		
RhB	1.354 x 10 ⁻² min ⁻¹	7.582 x 10 ⁻² min ⁻¹	6.43 x 10 ⁻² min ⁻¹		
	$(2.225 \times 10^{-4} \text{ s}^{-1})$	$(12.46 \times 10^{-4} \text{ s}^{-1})$	$(10.56 \times 10^{-4} \text{ s}^{-1})$		
CR	1.471 x 10 ⁻² min ⁻¹	8.23 x 10 ⁻² min ⁻¹	6.98 x 10 ⁻² min ⁻¹		
	$(2.45 \times 10^{-4} \text{ s}^{-1})$	$(13.72 \times 10^{-4} \text{ s}^{-1})$	$(11.63 \times 10^{-4} \text{ s}^{-1})$		

4 Role of scavengers

To recognize the active oxidative species involved in the photocatalytic removal of the dyes with the mesoporous materials, the scavenger experiment was performed. Ammonium oxalate (AO), tert-butyl alcohol (TBA), and N2 were used as scavengers for understanding the role of h⁺ (positive hole), hydroxyl radical (OH \bullet) and superoxide radicals (O $\vec{2}$ $\vec{\bullet}$) respectively towards the removal of the dyes. The same experiment was also conducted in the absence of these trapping agents and the combined results were shown in figure 11. N₂ purging restricts the oxidation of dyes, as it controls the liberation of the superoxide radical ions (O2-) [33]. TBA can inhibit the removal of dyes from its aqueous solution, as it can suppress the participation of the hydroxyl radicals (OH•) towards the destruction of the organic dyes [34]. Similarly, AO can arrest the activity of positive holes (h⁺) formed by the electronic excitation from the VB to CB in the mesoporous material [35]. In these studies, it was observed the removal tendency was less in the presence of these trapping agents. Nevertheless, under nonscavenger conditions (blank), the removal effectiveness was high, in both the dyes with the metal-MCM-41 mesoporous materials. Hence, it was concluded that the redox process was effective with both O2 and OH• species acting as active radicals for the removal of the dyes.

5 Probable mechanism

On illuminating the dye solutions with the photocatalyst, the electrons in the valence bond (VB) excite the conduction band (CB) and generate a positive hole (h⁺) and electron (e⁻) in VB and CB respectively, resulting in the generation of the e⁻/h⁺ pairs. They may recombine and could decrease the availability of the charges for the redox process to occur. This recombination could be controlled by a photocatalyst whose bandgap is narrow, and hence contributes to the generation of the redox-active species, superoxide radical ion, and hydroxyl radicals. In this regard, the Mn & Al-MCM-41 mesoporous materials possess a narrow band gap, as observed in the UV-Vis DRS analysis and, enhance the oxidation of the RhB and CR dyes effectively as shown in equations (6) to (12).

$$\begin{array}{lll} M - MCM - 41 + h\nu \rightarrow M - MCM - 41(h^{+} + e^{-}) & (6) \\ M = Mn^{3+}, Al^{3+} & & (7) \\ O_{2} + e^{-} \rightarrow O_{2}^{\bullet} & (7) \\ O_{2}^{\bullet \bullet} + H^{+} \rightarrow HO_{2}^{\bullet} & (8) \\ 2HO_{2}^{\bullet} \rightarrow O_{2} + H_{2}O_{2} & (9) \\ H_{2}O_{2} + O_{2}^{\bullet \bullet} \rightarrow OH^{\bullet} + OH^{-} + O_{2} & (10) \\ H_{2}O_{2} + h\nu \rightarrow 2OH^{\bullet} & (11) \\ O_{2}^{\bullet \bullet}/OH^{\bullet} + Rhb/CR \rightarrow Degradation Products & (12) \\ \end{array}$$

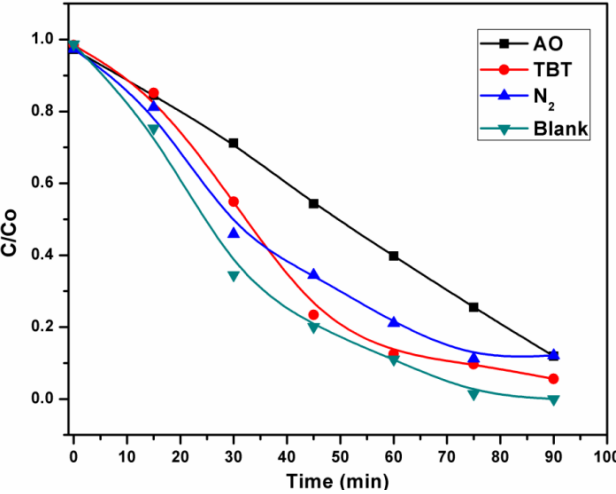


Figure 11: Role of scavengers in the photocatalytic action of Mn & Al-MCM-41

In general, mesoporous silica (MCM-41) possesses a regular honeycomb structure with uniform cylindrical pores with pore sizes in the range of 15 to 100 A° [3]. It shows the existence of a large surface area, which increases the rate of adsorption on its surface and enhances the removal rate. Secondly, the dimeric species formation would be controlled in the aqueous solution in its presence. This condition arrives due to the higher adsorbing tendency of the MCM-41 materials, immobilized with metal ions. These two factors arise mainly due to the incorporation of the metal ions into the framework of the mesoporous silica [37].

6 Conclusions

This research protocol brings out a facile synthesis of Mn and Al incorporated MCM-41 mesoporous materials through the coprecipitation method. They were characterized and proved their mesoporosity, sufficient surface area, and higher absorption wavelengths in the visible region. The insertion of the Mn⁺³ and Al⁺³ ions into MCM-41 material was clearly seen from these results. Based on their visible light active nature, their photocatalytic ability was examined towards the removal of RhB and CR dyes. It was observed that the removal tendency was slightly more with Mn-MCM-41 than with the Al incorporated mesoporous material. The removal tendency was observed to be due to the superoxide radical ion and the hydroxyl radicals and the kinetic profiles revealed the existence of first-order kinetics on applying the L-H kinetic model.

Acknowledgment

The authors are thankful to the Advanced Analytical Laboratory, Andhra University, Visakhapatnam (AP, India) for providing the results of XRD, FESEM-EDX, and FTIR analysis, Sophisticated instrumentation facility (SIF), IIT Madras for providing the analysis results of BET surface area and UV-Vis DRS techniques.

Ethical issue

Authors are aware of and comply with, best practices in publication ethics specifically with regard to authorship (avoidance of guest authorship), dual submission, manipulation of figures, competing interests, and compliance with policies on research ethics. Authors adhere to publication requirements that submitted work is original and has not been published elsewhere in any language.

Competing interests

The authors declare that no conflict of interest would prejudice the impartiality of this scientific work.

Authors' contribution

All authors of this study have a complete contribution for data collection, data analyses and manuscript writing.

References

- 1. Beck JS, US Patent 5057296 (1991).
- Kresge CT, Leonowicz, ME, Roth, WJ, Vartuli, JC, Beck JS, Ordered mesoporous molecular sieves synthesized by a liquid-crystal template mechanism, Nature 1992; 359: 710-712. doi.org/10.1038/359710a0
- Beck JS, Vartuli JC, Roth, WJ, Leonowicz, ME, Kresge CT, Schmitt KD, Chu CTW, Olson DH, Sheppard EW, McCulle SB, Higgins JB, Schlender, JL, A new family of mesoporous molecular sieves prepared with liquid crystal templates, J. Am. Chem. Soc. 1992; 114: 10834-10843. doi.org/10.1021/ja00053a020.
- Zhao XS, Lu GQ, Millar, GJ, Advances in mesoporous molecular sieves, Ind. Eng. Chem. Res. 1996; 35 (7): 2075-2090. doi.org/10.1021/ie950702a.
- Mercier L, Pinnavaia TJ, Access in mesoporous materials: advantages of a uniform pore structure in the design of a heavy metal ion adsorbent for environmental remediation, Adv. Mater. 1997; 9(6): 500-503. doi.org/10.1002/adma.19970090611.
- Corma A, From microporous to mesoporous molecular sieve materials and their use in catalysis, Chem. Rev. 1997; 97 (6): 2373-2420. doi.org/10.1021/cr960406n.
- Karthik M, Tripathi AK, Gupta NM, Vinu A, Hartmann M, Palanichamy M, Murugesan V, Characterization of Co, Al-MCM-41 and its activity in the t-butylation of phenol using isobutanol, Applied Catalysis A: General 2004; 268 (1-2): 139–149.
- Tanev PT, Chibwe M, Pinnavaia, TJ, Titanium containing mesoporous molecular sieves for catalytic oxidation of organic compounds, Nature 1994; 368: 321-323. doi.org/10.1038/368321a0.
- Tuel A, Modification of mesoporous silicas by incorporation of hetero atoms in the frame work, Micropor. Mesopor. Mater. 1999; 27 (2-3): 151-169. doi.org/10.1016/S1387-1811(98)00250-9.
- Lim S, Haller, GL, Gas phase methanol oxidation on VMCM-41, Appl. Catal. A: Gen. 1999; 188 (1-2): 277-286. doi:10.1016/S0926-860X(99)00213-6
- Selvaraj M, Sinha PK, Lee K, Ahn I, Pandurangan A, Lee TG, Synthesis and characterization of Mn-MCM-41 and Zr-Mn-MCM-41, Micropor. Mesopor. Mater. 2005; 78 (2-3): 139–149. doi.org/10.1016/j.micromeso.2004.10.004

- Kefu Z, Xiao DX, Chang TC, Photocatalytic degradation of tetracycline by Ti-MCM-41 prepared at room temperature and biotoxicity of degradation products, App. Surf. Sci. 2017; 416: 248-258. doi.org/10.1016/j.apsusc.2017.04.174.
- Luan L, Cheng CF, Zhou W, Klinowski J, Mesopore molecular sieve MCM-41 containing framework aluminum, J. Phys. Chem. 1995; 99 (3): 1018-1024. doi.org/10.1021/j100003a026.
- Mokaya R, Jones W, Acidity and catalytic activity of aluminosilicate mesoporous molecular sieves prepared using primary amines, J. Chem. Soc. Chem. Commun. 1996; 8: 983-984. doi.org/10.1039/CC9960000983.
- Schmidt R, Akporiaye D, Stocker M, Ellestad OH, Synthesis of a mesoporous MCM-41 material with high levels of tetrahedral Aluminum, J. Chem. Soc. Chem. Commun. 1994; 12: 1493-1494. doi.org/10.1039/C39940001493.
- Selvaraj M, Pandurangan A, Seshadri KS, Sinha PK, Krishanasamy V, Lal KB, Comparison of mesoporous Al-MCM-41 molecular sieves in the production of cumene for isopropylation of toluene, J. Mol. Cata. A. Chem. 2002; 186(1-2): 173-186. doi.org/10.1016/S1381-1169(02)00134-6.
- Zhao D, Goldfarb D, Synthesis of mesoporous manganosilicates: Mn-MCM-41, Mn-MCM-48, Mn-MCM-L, J. Chem. Soc. Chem. Commun. 1995: 875-876. doi.org/10.1039/C39950000875.
- 18. Vetrivel S, Pandurangan A, Side-chain oxidation of ethylbenzene with *tert*-butylhydroperoxide over mesoporous Mn-MCM-41 molecular sieves, J. Mol. Catal. A. Chem. 2004; 217 (1-2): 165-174. doi.org/10.1016/j.molcata.2004.03.022.
- Vetrivel S, Pandurangan A, Vapour-phase oxidation of ethylbenzene with air over Mn-containing MCM-41 mesoporous molecular sieves, Appl. Catal. A. Gen. 2004; 264 (2): 243-252. doi.org/10.1016/j.apcata.2003.12.047.
- Pandurangan A, Vetrivel S, Anthea B, Catalytic oxidative transformation of benzyl alcohol and cyclohexanol over mesoporous Mn-MCM-41 and Mo-MCM-41 and Mo(Im), Mn-MCM-41 molecular sieves, Ind. J. Chem. Tech. 2004; 11 (2): 248-253.
- Zhang QH, Wang Y, Itsuki S, Shishido T, Takehira K, Manganese containing MCM-41 for epoxidation of styrene and stilbene, J. Mol. Catal. A. Chem. 2002; 188 (1-2): 189-200. doi.org/10.1016/S1381-1169(02)00323-0.
- 22. Ma HT, Yuan ZY, Wang Y, Bao XH, Temperature programmed surface reaction study on C₂-oxygenate synthesis over SiO₂ and nanoporous zeolitic material supported Rh-Mn catalysts, Surf. Inter. Anal. 2001; 32 (1): 224-227. doi.org/10.1002/sia.1042.
- 23. (a) Reddy KM, Moudrakovski I, Sayari A, Synthesis of mesoporous vanadium silicate molecular sieves, J. Chem. Soc. Chem. Commun. 1994; 1059-1060. doi:10.1039/C39940001059 (b) Guru TVSPVS, Krishna V, Rajesh E, Efficacy of cobalt-incorporated mesoporous silica toward photodegradation of Alizarin Red S and its kinetic study, J. Chin. Chem. Soc. 2020; 68 (4): 592-600. doi: 10.1002/jccs.202000335.
- Ma Y, Tong W, Zhou H, Suib SL, A review of zeolite-like porous materials, Micropor. Mesopor. Mater. 2000; 37 (1-2): 243-252. doi.org/10.1016/S1387-1811(99)00199-7.
- Zhao D, Huo Q, Feng J, Chmelka BF, Stucky GD, Nonionic Triblock and Star Diblock Copolymer and Oligomeric Surfactant Syntheses of Highly Ordered, Hydrothermally Stable, Mesoporous Silica Structures, J. Am. Chem. Soc. 1998; 279 (5350): 548-552.
- Petrini G, Cesana A, Alberti G De, Geroni F, Leofanti G, Padovan M, Paparatto G, Rofia P, Deactivation phenomena on Ti-Silicalite, Stud. Surf. Sci. Catal. 1991; 68: 761-766. doi.org/10.1016/S0167-2991(08)62710-X.
- Selvaraj M, Hoo KB, FTIR studies on selected mesoporous metallosilicate molecular sieves, Chem. Lett. 2005; 34 (9): 1290-1291. doi.org/10.1246/cl.2005.1290.
- 28. Czaja M, Lisiecki R, Chrobak A, Sitko R, Mazurak Z, The absorption- and luminescence spectra of Mn³+ in beryl and vesuvianite, Phy. Chem. of Mat. 2018; 45: 475-488. doi.org/10.1007/s00269-017-0934-x.

- Sekhar RS, Douglas SP, Graphene oxide–nano-titania composites for efficient photocatalytic degradation of indigo carmine, J Chin Chem Soc. 2018; 65 (12): 1423-1430. doi.org/10.1002/jccs.201800154
- Birtalan E, Rudat B, Kolmel DK, Fritz D, Vollrath SB, Schepers U, Brase S, Investigating Rhodamine B –labeled peptoids: scopes and limitations of its applications. Biopolymers, 2011; 96 (5): 694-701. doi.org/10.1002/bip.21617.
- Sekhar RS, Douglas SP, Efficient Removal of Nitrogen based Industrial Pollutants by Graphene Oxide Coupled Nanotitania Composite under Visible Light Illumination, J. Environ. Treat. Tech. 2021; 9(1): 183-191. doi.org/10.47277/JETT/9(1)191.
- Ozkan A, Ozkan MH, Gurkan R, Akcay M, Sokmen M Photocatalytic degradation of a textile azo dye, Sirius Gelb GC on TiO₂ or Ag-TiO₂ particles in the absence and presence of UV irradiation: the effects of some inorganic anions on the photocatalysis, J. Photochem. Photobiol. A, 2004; 163 (1-2): 29-35. doi.org/10.1016/S1010-6030(03)00426-X.
- 33. Kumar S, Surendar T, Baruah A, Shanker V, Synthesis of novel and stable g-C₃N₄-Ag₃PO₄ hybrid nanocomposite photocatalyst and study of the photocatalytic activity under visible light irradiation, J. Mater. Chem. A, 2013; 1 (17): 5333–5340. doi.org/10.1039/C3TA00186E.
- 34. Liu T, Wang L, Lu X, Fan J, Cai X, Gao B, Miao R, Wang J, Yongtao L, Comparative study of the photocatalytic performance for the degradation of different dyes by ZnIn₂S₄: adsorption, active species, and pathways, RSC Adv., 2017; 7: 12292-12300. doi: 10.1039/C7RA00199A
- Kumar S, Baruah A, Surendar T, Kumar B, Shanker V, Sreedhar B, Cost-effective and eco-friendly synthesis of novel and stable N-doped ZnO/g-C₃N₄ core-shell nanoplates with excellent visible-light responsive photocatalysis, Nanoscale, 2014; 6: 4830–4842. doi.org/10.1039/C3NR05271K.
- C.C. Leznoff, A.B.P. Lever, Vol. 1, VCH, New York, NY, 1989, p. XII.